

Controllable drug release and simultaneously carrier decomposition of SiO₂-drug composite nanoparticles

Silu Zhang, Zhiqin Chu, Chun Yin, Ge Lin, and Quan Li

J. Am. Chem. Soc., **Just Accepted Manuscript** • DOI: 10.1021/ja3123015 • Publication Date (Web): 18 Mar 2013

Downloaded from <http://pubs.acs.org> on March 27, 2013

Just Accepted

“Just Accepted” manuscripts have been peer-reviewed and accepted for publication. They are posted online prior to technical editing, formatting for publication and author proofing. The American Chemical Society provides “Just Accepted” as a free service to the research community to expedite the dissemination of scientific material as soon as possible after acceptance. “Just Accepted” manuscripts appear in full in PDF format accompanied by an HTML abstract. “Just Accepted” manuscripts have been fully peer reviewed, but should not be considered the official version of record. They are accessible to all readers and citable by the Digital Object Identifier (DOI®). “Just Accepted” is an optional service offered to authors. Therefore, the “Just Accepted” Web site may not include all articles that will be published in the journal. After a manuscript is technically edited and formatted, it will be removed from the “Just Accepted” Web site and published as an ASAP article. Note that technical editing may introduce minor changes to the manuscript text and/or graphics which could affect content, and all legal disclaimers and ethical guidelines that apply to the journal pertain. ACS cannot be held responsible for errors or consequences arising from the use of information contained in these “Just Accepted” manuscripts.



1
2
3 **Controllable drug release and simultaneously carrier decomposition of SiO₂-drug**
4 **composite nanoparticles**
5
6

7
8
9 Silu Zhang¹, Zhiqin Chu¹, Chun Yin², Ge Lin^{2*}, Quan Li^{1*}
10

11
12 ¹Department of Physics, The Chinese University of Hong Kong, Shatin, New Territories,
13
14 Hong Kong
15

16
17 ²School of Biomedical Sciences, Faculty of medicine, The Chinese University of Hong
18
19 Kong, Shatin, New Territories, Hong Kong
20
21
22
23
24
25
26
27
28
29

30 **ABSTRACT**
31

32
33 Drug release simultaneously with carrier decomposition has been demonstrated in
34
35 SiO₂-drug composite nanoparticles. By creating a radial drug concentration gradient in
36
37 the nanoparticle, controllable release of the drug is primarily driven by diffusion. Escape
38
39 of the drug molecules then triggers the SiO₂ carrier decomposition, which starts from the
40
41 center of the nanoparticle and eventually leads to its complete fragmentation. The small
42
43 size of the final carrier fragments enables their easy excretion via renal systems.
44
45
46 Together with the known biocompatibility of SiO₂, the feature of controllable drug
47
48 release and simultaneous carrier decomposition achieved in the SiO₂-drug nanoparticles
49
50 make it ideal for a wide range of diagnostic and therapeutic applications with great
51
52 promise for potential clinical translation.
53
54
55
56
57
58
59
60

INTRODUCTION

An ideal nanoparticle (NP) carrier-drug system has several features, including effective cellular uptake, controllable release, and safe excretion from the biological system after functioning. Improved cellular uptake has been claimed in several NP carrier-drug systems,¹⁻⁶ in which the drug molecules can be disguised by residing inside the carrier, while the carrier surface is hydrophilic for easy cellular uptake. Controllable release (with a desired releasing rate and duration) of the drug molecules from the carrier guarantees relatively stable therapeutic levels during the treatment period.⁷ Nevertheless, this task remains challenging in most of the NP carrier-drug systems. Elimination of the drug/drug carriers from the biologic system after their carrying out the diagnostic or therapeutic functions is another important aspect to consider. Unfortunately, this remains as one of the major obstacles impeding potential clinical translation of NP carrier-drugs. It has been found that the hydrodynamic size required for renal clearance is too small (<5.5nm⁸) to enable the incorporation of adequate amount of multifunctional components (e.g. for targeting, therapy etc.), and rapid renal excretion reduces the time available to the NPs to carry out its function. On the other hand, although materials of larger sizes (e.g. ~20-200nm) may provide host spacious enough for functionality loading and have prolonged residence time in the blood stream, they avoid renal filtration, leading to increased toxicity at system level.^{9,10} A most desirable design for improving the biocompatibility of NP carrier-drug would involve the incorporation of controllable drug release together with carrier self-destruction, through which carrier could be hierarchically degraded into harmless, renally clearable products^{11,12} after the drug carrying out their function.

1
2
3 Silica NPs are considered as one of the most promising carrier systems as it is
4 generally accepted as non-toxic,^{13,14} and provide a versatile platform for drug loading.¹⁵
5
6 The surface of the SiO₂ NP is hydrophilic, being favorable for cellular uptake. Three
7
8 generic strategies have been developed for drug loading into the SiO₂ NP carrier, i.e.,
9
10 with the drug molecules being embedded in the dense SiO₂ NPs, residing in the pores of
11
12 mesoporous SiO₂ NPs (MSN) and being attached on the surface of the NPs, via chemical
13
14 bonding or physical adsorption.^{4,16-19} Moderate success in drug release has been achieved
15
16 in some systems, when the gradual release of drug is controlled by morphological
17
18 characteristics of the NP carriers. For example, release of drugs has been reported via
19
20 diffusion using MSN with various pore morphologies.²⁰ Alternatively drug release
21
22 triggered by diverse physical and chemical stimuli has been realized via gated
23
24 mechanisms on mesoporous scaffolds. In the gated MSN, the pores loaded with guest
25
26 molecules are capped by nanoparticles via a cleavable linkage, by deformable polymers,
27
28 or by chemical molecules/ biomolecules. The guest molecules can then be released by
29
30 removing the caps via external stimuli such as photon, thermal or pH changes etc.²¹⁻²⁵
31
32 Nevertheless, none of these configurations can simultaneously satisfy the above three
33
34 criteria, in particular, the controlled release and carrier self-destruction to very small
35
36 sized fragments are highly desired but not realized.
37
38
39
40
41
42
43
44
45

46 In the present work, we have developed a special type of SiO₂-drug composite
47
48 NPs by introducing drug molecules into SiO₂ during the NP growth at controlled
49
50 experimental conditions. Taking methylene blue (MB) as an example, we show that by
51
52 creating a radial concentration gradient of MB in the NP, MB release occurs
53
54 simultaneously with the SiO₂ carrier decomposition, as driven by drug molecule diffusion.
55
56
57
58
59
60

1
2
3 The key factors that determine the specific MB release and SiO₂ carrier decomposition
4 characteristics are identified. The experimental results suggest a most attractive and
5
6 promising NPs carrier-drug system for diagnostic and therapeutic applications. We also
7
8 shown that such simple growth mechanism can be applied to many other molecules
9
10 employing the SiO₂ NP carrier, with the same feature achieved.
11
12
13
14
15
16
17
18

19 RESULTS AND DISCUSSION

20
21
22 **Characterization of SiO₂-MB NPs.** Figure 1a showed a typical transmission
23 electron microscopy (TEM) image of the as-synthesized silica-MB NPs. They were
24 spherical in shape with an average diameter of ~80 nm. Successful incorporation of the
25 MB into the NPs was suggested by the absorption spectrum taken from the NP sample.
26
27 Compared to the pure MB absorption measured in aqueous solution, its characteristic
28 absorption at ~665 nm (for monomer absorption) and ~600 nm (for dimer absorption)
29
30 were clearly observed in the SiO₂-MB NP sample, but not in the control sample
31
32 containing pure SiO₂ NPs (Figure 1b). The relatively higher intensity of the dimer
33
34 absorption peak (as compared to the monomer one) indicated aggregation of MB
35
36 molecules, which occurred when they were grown into the SiO₂ NPs.¹⁶ This served as an
37
38 additional piece of evidence that MB resided inside the SiO₂ NPs.
39
40
41
42
43
44
45
46
47
48

49 Further evidence of MB incorporation and information on their spatial distribution
50 inside the NP were provided by chemical maps obtained using electron energy loss
51 spectroscopy (EELS). Figure 1c-e gave the filtered bright field TEM image of one such
52
53 NP and the corresponding chemical maps taken from two compositional elements—Si
54
55
56
57
58
59
60

1
2
3 and N (a major compositional element of MB). Non-uniform distribution of both Si and
4
5 N was observed, i.e., N was found to be more concentrated in the center of the NP,
6
7 whereas Si was deficient. By removing the thickness contribution in the elemental
8
9 mapping, the abundance profile of N was obtained, in which one can see a decreasing N
10
11 amount from the center to the surface of the NPs (Supporting information Figure S1a).
12
13 Further evidence on the feature of “central concentrated MB” was obtained by calcination
14
15 of the NPs at elevated temperatures, when the MB molecules were removed and center-
16
17 hollow SiO₂ NPs were obtained (Supporting information Figure S1b).
18
19
20
21
22

23 **Controllable drug release and simultaneously carrier decomposition of SiO₂-**
24 **MB NPs.** Absorption spectra were taken from both the NPs (dried and then re-dispersed
25
26 in water) (Figure 2a) and the supernatant (Figure 2b) of sample M1 (with MB loading
27
28 amount as 75 μg MB / mg NP), after the NPs had been immersed in deionized water for
29
30 specified period of times (2 hours, 1, 2, 3, 6, 9, and 14 days) at room temperature. The
31
32 released chemical in the supernatant has two characteristic absorptions at ~665 nm and
33
34 ~600 nm, which agree with the monomer and dimer absorption of MB, respectively. This
35
36 result suggests the chemical integrity of MB when being encapsulated into the silica NPs
37
38 (Further evidence from high performance liquid chromatography (HPLC) can be found in
39
40 Supporting information Figure S2). Figure 2c respectively plotted the profiles of the
41
42 amount of MB released from NPs and those remained in NPs as a function of time (i.e.,
43
44 evolution of the MB absorption peak intensity from both supernatant and NPs within the
45
46 testing period). A decrease of MB absorption in the NPs occurred simultaneously with an
47
48 increase of that in the supernatant, suggesting the release of MB from NP to the solution.
49
50 An interesting feature observed in the absorption spectra of the NPs was the intensity
51
52
53
54
55
56
57
58
59
60

1
2
3 variation of the monomer and the dimer absorption peaks, the ratio evolution of the two
4 was plotted in Figure 2d. With less and less MB being left in the NPs, the monomer
5
6
7
8 absorption started to take the lead, while the dimer absorption dominated at the beginning
9
10
11 for the as-synthesized NP. In fact, the dominance switching from dimer to monomer can
12
13 be controlled to occur at different time points, by adjusting the initial MB and tetraethyl
14
15 orthosilicate (TEOS) amount during NP growth (Supporting information Figure S3).
16
17

18
19 In order to simulate in-vivo situations, we have also carried out two sets of
20
21 experiments. In the first one, we compared the drug release in phosphate buffered saline
22
23 (PBS) at 37°C at two different pH value, i.e. pH~7.4 (normal physiological conditions)
24
25 and ~5 (intracellular conditions of cancer cells), respectively. Our results showed that the
26
27 drug release from the NPs was faster at pH~7.4 in the first 24 hours, but became slower
28
29 than that at pH~5 afterwards (Figure 2e). In the second set of experiments, the pH was
30
31 controlled ~7.4, and PBS or serum was used as medium for the inspection of drug release
32
33 from the NPs. A lower drug release rate was obtained in serum than in PBS (Figure 2f),
34
35 likely due to the protein coating absorbed on the surface of NPs when using serum as the
36
37 medium.
38
39
40
41
42

43 The corresponding morphological evolution of the SiO₂-MB NPs (sample M1)
44
45 was recorded using TEM (Figure 3a-d). Most of the NPs remained intact at day 1, while
46
47 obvious hollow feature appeared in the center of many of the NPs after 4 days immersion.
48
49 Such center-hollow feature continued to enlarge in the following days, leaving a spherical
50
51 shell of SiO₂ with thinner and thinner shell thickness. At day 9, some of the nanoshells
52
53 appeared as partially damaged (marked by arrows in Figure 3c), and even longer duration
54
55 (after 10 days) led to complete collapse of the nanoshell structure to scattered fragments
56
57
58
59
60

1
2
3 (Figure 3d), coinciding with the MB releasing pattern suggested by the time dependent
4 absorption spectra (Figure 2). In fact, over 95% of the Si (from fragmented SiO₂ NPs)
5 was found in the supernatant after their 14 days immersion in deionized water (Figure 3e).
6
7
8 The decomposition profile (as measured by the Si amount in the supernatant) of the SiO₂-
9 MB NPs was also examined at pH 7.4 in PBS at 37°C (Figure 3f) and in simulated body
10 fluid at 37 °C (Figure 3g). The NP decomposition was found to occur the fastest in PBS,
11 and the slowest in deionized water.
12
13
14
15
16
17
18
19

20
21 Release of MB from the SiO₂ NP carrier were also inspected in vitro. After being
22 incubated with the SiO₂-MB NPs for a certain period of time, cell samples were examined
23 by both confocal microscopy and TEM. Cellular uptake of the NPs were confirmed by the
24 MB fluorescence signal in the cells (Figure 4a), after their being incubated with the NPs
25 for 24 hours. The NPs were known to enter the cell interior via endocytosis,²⁶ a direct
26 consequence of which was the NPs' residing in membrane bounded vesicles as
27 aggregates (Supporting information, Figure S4). As a result, the concentrated MB
28 fluorescence signal observed in a randomly spotted pattern in the cells (Figure 4a,b)
29 suggested that most of the MB molecules were confined inside the NPs at the end of 24
30 hours incubation. Similar results (Supporting information, Figure S6a,b) were obtained
31 when using dense SiO₂ NPs containing MB (in which MB is known to be stably confined
32 within the dense SiO₂ NP carrier. Basic characterizations of the dense SiO₂-MB NPs can
33 be found in the supporting information Figure S5). Although both types of NPs (self-
34 decomposable vs. dense) were amorphous in nature, porosimetry measurement showed
35 that the self-decomposable NPs were characterized by larger surface area (45.404 m²/g)
36 and pore volume (0.3239 ml/g), in comparison with those of the dense NPs (surface area
37
38
39
40
41
42
43
44
45
46
47
48
49
50
51
52
53
54
55
56
57
58
59
60

1
2
3 16.787 m²/g and pore volume 0.0787 ml/g). 48 hours incubation of cells respectively with
4
5 the two types of NPs (the dense one and self-decomposable one) disclosed an intriguing
6
7 difference between the two cell samples. The spotted fluorescence pattern remained in
8
9 dense SiO₂-MB NP treated cells, and a stronger intensity was observed (Supporting
10
11 information, Figure S6c,d), due to continuous uptake of NPs by the cell during the
12
13 prolonged incubation period. As a comparison, most of the concentrated fluorescence
14
15 spots in the self-decomposable SiO₂-MB NP treated cells faded, while a rather diffusive
16
17 fluorescence background was observed, with intense fluorescence spots only
18
19 occasionally found (Figure 4c,d). A reasonable explanation to the experimental
20
21 observation was that MB escaped from the NPs, and was eventually released to
22
23 cytoplasm. The release of MB in vitro was also measured quantitatively. We had
24
25 respectively incubated the cells with self-decomposable SiO₂-MB NPs and dense SiO₂-
26
27 MB NPs for two different durations (i.e., 24 hours and 48 hours), and compared the
28
29 amount of MB released to the cytoplasm per cell. A striking difference between the cells
30
31 treated with the self-decomposable and dense SiO₂-MB NPs can be observed, i.e, the
32
33 amount of MB released from the self-decomposable NPs was an order of magnitude
34
35 higher than that of the dense ones (Figure 4e). Further support of the MB release pattern
36
37 came from TEM, as one can find that NPs remain in the endo/lysosome, but become
38
39 porous/shell like as MB escaped (Supporting information Figure S7).
40
41
42
43
44
45
46
47
48

49 The MB release/SiO₂ decomposition rate can be manipulated by controlling the
50
51 source MB concentration during the NP growth. Figure 5 compared the morphology
52
53 evolution of three SiO₂-MB NP samples (M1, M2, and M3 with MB loading amount as
54
55 75μg MB / mg NP, 110μg MB / mg NP and 230μg MB / mg NP, respectively.) After
56
57
58
59
60

1
2
3 being dispersed in deionized water for two days, the morphology of sample M1 was
4
5 hardly changed with only small hollow features emerging from the center of the NPs.
6
7 When the initial MB concentration was higher (sample M2), distinct nanoshell structures
8
9 were observed after two days. Further increase in the initial MB concentration (sample
10
11 M3) resulted in slightly different morphology for the as-synthesized NPs, i.e., the
12
13 aggregated MB molecules in the center of the NPs gave brighter contrast in the TEM
14
15 image (Figure 5e) due to its lower mass thickness as compared to that of SiO₂. At the end
16
17 of two days, completely rupture of many NPs was observed, in addition to the hollow
18
19 nanoshells with very thin shell thickness.
20
21
22
23
24

25
26 **Drug release and carrier decomposition mechanism.** The above experimental
27
28 results suggested possible control over the drug release with simultaneously carrier
29
30 decomposition, which was driven by a diffusion controlled mechanism. The radial MB
31
32 concentration gradient from inner out served as a major driving force for MB release. The
33
34 center-out-first releasing pattern was primarily determined by the growth characteristic of
35
36 MB molecules within the SiO₂ NPs. At the beginning of the synthesis, very small amount
37
38 of silica species presented, as they were not directly added as source chemicals, but
39
40 produced from the TEOS hydrolysis. As a comparison, MB was directly added as the
41
42 source molecules, so its concentration was the highest at the start of the synthesis. In the
43
44 presence of small amount of silica species, MB molecules were then driving to aggregate
45
46 (Supporting information Figure S8) due to the opposite charge of MB and silica species
47
48 (the later serving as “glue” for MB molecule aggregation).²⁷ These aggregated MB
49
50 molecules (entangled with very small amount of silica species) became the “nuclei” for
51
52 further growth of SiO₂-MB NP. As the TEOS hydrolysis persisted and NP growth
53
54
55
56
57
58
59
60

1
2
3 process proceeded, more and more silica species were produced, while the MB source
4 was continuously consumed as the NP got larger. With such a pattern, high MB
5 concentration occurred in the center of the NPs, agreeing well with the experimentally
6 observed spatial distribution of the compositional elements. A key factor for the
7 formation of “MB-rich nuclei” was the maintenances of high MB concentration and low
8 silica species (from TEOS hydrolysis) concentration at the beginning of the growth.
9 Experimentally, one can either choose to use high MB initial concentration (ranged from
10 85 μ M to 850 μ M in the present case), or limit the silica species initial concentration (by
11 controlling the TEOS hydrolysis rate) to form the “MB-rich nuclei” and obtain the self-
12 decomposable NPs. The latter can be done by adjusting the ammonia amount, which was
13 controlled at <1.08%vol. in the present case. When such conditions were not satisfied,
14 one obtained dense NPs, which was commonly reported in the literature.¹⁶
15
16
17
18
19
20
21
22
23
24
25
26
27
28
29
30
31

32
33 To support the diffusion controlled mechanism, we carried out another control
34 experiment, i.e., by dispersing the SiO₂-MB NPs into benzene, in which MB was not
35 soluble, neither the MB release nor the SiO₂ NP decomposition occurred (Supporting
36 information, Figure S9). In fact, the SiO₂-MB NP was very stable after being dried—
37 neither MB escape nor SiO₂ decomposition occurred after months when they were stored
38 in the powder form.
39
40
41
42
43
44
45
46

47
48 Chemical reaction between the SiO₂ and the MB can be completely ruled out
49 (Supporting information Figure S10) as a possible reason for SiO₂ carrier decomposition.
50 Such decomposition was triggered by the out-escaping of MB molecules. The
51 decomposition started from the center of the NPs, as suggested by the time dependent
52 morphological change of the NPs, when they were dispersed in MB soluble solvent
53
54
55
56
57
58
59
60

1
2
3 (Figure 3). This was reasonable as the center of the NP was mainly composed of high
4 concentration MB with little SiO₂ incorporated, so that the carrier “bone” structure was
5 the most vulnerable in the center. As MB molecules continuously moved out of the NPs,
6
7
8
9
10 the SiO₂ “network” (as they grow together with the MB during NP formation) was
11
12
13 damaged, eventually led to complete collapse of the NPs when all drug molecules were
14
15 released. Consequently, the higher MB concentration in the source material during NP
16
17 growth, the faster the release of the MB and decay of the SiO₂ carrier (Figure 5).
18
19
20 Eventually the carriers completely dissolved into small enough species, which content is
21
22 biologically benign. The urine of rats were collected at different time points after
23
24 injection of SiO₂-MB NPs (Sample M4), and the Si amount were detected by ICP-OES
25
26 (Figure 6a). This in vivo result showed a significant amount of Si excretion via urine
27
28 using the self-decomposable SiO₂-MB NPs, as compared to that using dense SiO₂-MB
29
30 NPs. Consistent results were obtained in the biodistribution study of the NPs. Similar to
31
32 many other nanomaterials,²⁸⁻³⁰ the injected SiO₂-MB NPs accumulated mainly in the
33
34 mononuclear phagocytic system-related organs such as the liver and the spleen (Figure
35
36
37 6b). However, the self-decomposable SiO₂-MB NPs had a significantly lower
38
39 accumulation amount in the corresponding organs compared to those of dense SiO₂-MB
40
41 NPs at 48 hours after injection. This was attributed to their easy degradation followed by
42
43 fast excretion via renal system.
44
45
46
47
48

49
50 Such self-decomposing mechanism can be applied to many different SiO₂-carrier
51
52 NP systems. Here we gave a few additional examples. Different dye molecules (such as
53
54 Oxazine725 and LDS751) had been incorporated into the SiO₂ NPs and similar dye
55
56 release and carrier decomposition had been observed (Supporting information Figure
57
58
59
60

1
2
3 S11). In addition, we had also incorporated a different drug molecule, i.e., Doxorubicin
4 (Dox), into the SiO₂ NPs. Figure 7a showed the optical absorption of such NPs. The
5
6 characteristic absorption peak of Dox at ~490nm can be observed from the NPs dispersed
7
8 in aqueous solution, suggesting successful loading of the drug into the NPs. The release
9
10 profile of Dox from the NPs (pH 7.4 PBS at 37°C) was shown in Figure 7b. The
11
12 cumulative release of Dox could reach ~75% within 7 days at the present loading
13
14 concentration (72 μg Dox / mg NP).
15
16
17
18
19
20

21 Release of Dox from the self-decomposable NPs was also visualized using
22
23 confocal microscopy. After being incubated with such NPs for a certain period of time
24
25 (24 hours and 48 hours), the intracellular distribution of the NPs and the Dox release
26
27 were examined using Dox fluorescence signal in the range of 550nm~625nm (excited by
28
29 using 476nm laser). Concentrated Dox fluorescence signal was observed in a randomly
30
31 spotted pattern in the cells, suggesting that most Dox molecules were confined inside the
32
33 NPs (which were in the endo/lysosomes) at the end of 24 hours incubation (Figure 7c, d).
34
35 After another 24 hours (i.e., the 48 hours time point), most of the concentrated
36
37 fluorescence spots faded, while a rather diffusive fluorescence background was observed,
38
39 (Figure 7e, f) indicating that the Dox molecules escaped from the NPs, and were
40
41 eventually released to cytoplasm. This pattern was similar to that of the MB release. The
42
43 amounts of Dox released in the cells were also determined quantitatively (Figure 7g).
44
45
46
47
48
49

50 On the other hand, the corresponding decomposition of such NPs was illustrated
51
52 by the morphological evolution of NPs using TEM images taken as a function of time
53
54 (Figure 8). One can observe that hollow feature starts from the center of the NP,
55
56
57
58
59
60

1
2
3 eventually leading to complete fragmentation of the NP, being identical to that of the
4
5 SiO₂-MB NPs.
6
7
8
9

10 11 12 **CONCLUSION**

13
14
15 In conclusion, controlled release and carrier decomposition can be simultaneously
16 realized using a special type of SiO₂ carrier-drug composite NPs. A structural feature of
17 the NP carrier-drug is that the drug molecules are highly concentrated in the NP center
18 and a loose SiO₂ network is entangled with the drug molecule in the NP. Drug release is
19 primarily determined by diffusion, and further triggers the SiO₂ carrier decomposition.
20 This unique feature would enable the NP carrier drug avoid renal filtration at first,
21 leading to prolonged drug residence time in the blood stream. After complete release of
22 the drug, the carrier structure can be decomposed to small fragments for easy system
23 excretion. The model system of SiO₂-MB NPs is a simplest case in growth due to the
24 opposite charge between MB and the silica species. To incorporate neutral and/or
25 negatively charged molecules, one can either modify the interaction between the silica
26 species and the desired chemical molecules^{31,32,15}, or employ absorbing mechanism⁴ for
27 loading the neutral and/or negatively charged molecules into an existing self-
28 decomposable NP system. In this way, the present methodology can be generally applied
29 to a wide range of chemical molecules and opens a new direction for nanodrug design.
30
31
32
33
34
35
36
37
38
39
40
41
42
43
44
45
46
47
48
49
50
51
52
53
54

55 **EXPERIMENTAL SECTION**

56
57
58
59
60

1
2
3
4 **Synthesis and characterization of SiO₂-MB NPs.** The SiO₂-MB NPs were
5
6 synthesized using conventional method¹⁶ with modified parameters. In a typical
7
8 procedure, certain amount of MB (2.5mg for sample M1 and M4, 5mg for sample M2,
9
10 25mg for sample M3) was firstly added to a mixture of 75 ml ethanol with 3.4 ml 25%
11
12 (for M1, M2, M3) or 10% (for M4) ammonia-water solution, after that 0.08 ml TEOS
13
14 was added. The SiO₂-MB NPs were obtained after 24 hours' stirring, and washed several
15
16 times before their being dried. Doxorubicin, Oxazine725 and LDS751 were incorporated
17
18 into self-decomposable NP using similar strategies. The dense SiO₂-MB NPs were
19
20 synthesized using published method,¹⁶ briefly, 2.5 mg of MB was added to a mixture of
21
22 50ml ethanol with 5 ml 25% ammonia-water solution, after that 0.2 ml TEOS was added.
23
24 The ammonia amount is 2.27%vol., which is more than double of that in synthesizing
25
26 self-decomposable NPs (<1.08%vol.). Such recipe was known to generate dense SiO₂-
27
28 MB NP, in which the MB can be stably trapped in SiO₂.¹⁶
29
30
31
32
33
34

35 The general morphology and the size distribution of the NPs were characterized
36
37 using transmission electron microscopy (TEM, PhilipsCM120). The electron energy-loss
38
39 spectroscopy (EELS) was performed in TEM (Tecnai G2, FEG) attached with a Gatan
40
41 imaging filtering (GIF) system. The chemical maps of the compositional elements were
42
43 obtained at the Silicon L edge (at 99 eV), and Nitrogen K edge (at 401 eV). All of the
44
45 UV/Vis absorption spectra were acquired using HitachiU-3501 UV-visible-NIR
46
47 spectrophotometer.
48
49
50

51 **Characterizations of the drug release and carrier decomposition process.** The
52
53 MB release was first examined by dispersing the SiO₂-MB NPs (sample M1, 1mg/ml) in
54
55 10 ml deionized water, PBS or Serum (Fetal bovine serum, 50% in pH 7.4 PBS). A series
56
57
58
59
60

1
2
3 of aliquots (1 ml) of solution was removed at different time points and filtered with a
4 centrifugal filter (molecular weight cut off: 30000 Da, Millipore) to separate the NPs and
5 supernatant. The NPs were dried and re-dispersed in deionized water. UV/Vis absorption
6 spectra were taken from both redispersed particles solution and the supernatants using
7 HitachiU-3501 UV-visible-NIR spectrophotometer. The degradation of the SiO₂ carrier
8 was monitored by both morphology investigation using TEM and analysis of the above
9 supernatant using inductively coupled plasma optical emission spectrometer (ICP-OES,
10 PerkinEimer Optima 4300 DV).
11
12
13
14
15
16
17
18
19
20
21

22 In vitro experiments were conducted using H1299, human lung carcinoma cells,
23 which were cultured in RPMI 1640 medium, supplemented 10% heat-inactivated Fetal
24 bovine serum, 1% streptomycin and 1% penicillin. The cells were maintained in a
25 standard, cell culture incubator at 37°C in a humidified atmosphere with 5 % CO₂. All of
26 the NPs were sterilized by steaming at 115°C (NPs in powder form) for 2 hours and
27 dispersed in the medium by ultrasonication for at least 20 minutes right before their
28 introduction to the cells. Cells were seeded at initial densities of 5×10⁴ cells/mL in flasks
29 (for TEM samples) or dishes (for confocal samples) and incubated for 24 hours before
30 introducing NPs (sample M1), after that the original NP-free medium were discarded and
31 the fresh prepared NP-containing medium were added. Different cell “feeding time” was
32 adopted, as specified in individual experimental results.
33
34
35
36
37
38
39
40
41
42
43
44
45
46
47

48 Live NP-fed cells were used for confocal laser scanning microscopy (TCSP5,
49 Leica) with a 63 × water-immersion objective lens at 633 nm excitation and 650 nm -
50 700nm emission. For all transmission electron microscopy studies, the NP-fed cells were
51 fixed with typical procedures that can be found elsewhere.¹⁷ Microtome (Leica, EM UC6)
52
53
54
55
56
57
58
59
60

1
2
3 was then used to cut the cured cell cube (in Spurr resin (Electron microscopy sciences,
4 USA)) into thin slices (70-90 nm in thickness). The samples were collected on 300-mesh
5
6 copper TEM grids for observation.
7
8
9

10
11 For quantitative intracellular MB release experiment, the cells were incubated
12 with NPs for certain period and then were washed by PBS for several times and counted.
13
14 After that, the cells underwent lysis by freeze-thaw cycle, and were centrifugated (16000
15
16 \times g) to separate the released MB molecules (into the cytoplasm) from the residual NPs
17
18 (mainly existing as NP aggregates in the endo/lysosomes). The supernatants containing
19
20 the released MB molecules were collected and their optical absorptions were taken to
21
22 quantify the concentration of the released MB molecules. The average amount of the
23
24 released MB per cell was calculated by dividing total MB amount by the cell number.
25
26
27
28
29
30

31 **Urinary excretion and biodistribution of SiO₂-MB NPs.** For urinary excretion
32 investigation, Sprague-Dawley rats were randomly divided into two groups (n=3), and
33
34 injected with self-decomposable SiO₂-MB NPs, dense SiO₂-MB NPs (Sample M4, 40
35
36 mg/kg) or saline (control) through jugular vein cannula. The special single-rat metabolic
37
38 cages were used. The urine were collected into separate collection tubes at different time
39
40 points (4 hours, 12h hours, 24 hours, 36 hours and 48 hours) after injection. The urine
41
42 samples were then analyzed by ICP-OES for Si amount. For bio-distribution studies, the
43
44 rats were killed 48 hours after injection and the brain, heart, lung, liver, spleen and
45
46 kidney were collected. The tissues were digested and then analyzed for silicon content
47
48 using ICP-OES.
49
50
51
52
53
54
55
56
57
58
59
60

ASSOCIATED CONTENT**Supporting information**

Supporting figures, mainly including TEM image showing intracellular localization of NPs, characteristics of dense SiO₂-MB NPs, confocal images indicating evolution of the dense SiO₂-MB NPs in cells, TEM observation of carrier decomposition of SiO₂-MB NPs in cells, data of MB release and carrier decomposition in different solvents, test of the chemical reactivity between SiO₂ and MB, and data for extension of the synthetic methodology to other systems. This information is available free of charge via the internet at <http://pubs.acs.org>.

AUTHOR INFORMATION**Corresponding authors**

*E-mail: liquan@phy.cuhk.edu.hk; linge@cuhk.edu.hk

Notes

The authors declare no competing financial interest.

ACKNOWLEDGEMENTS

The authors are grateful to support from GRF of HKSAR (Project No. 414710) and SEG_CUHK06.

REFERENCES

- (1) Torchilin, V. P. *Nature Reviews Drug Discovery* 2005, 4, 145.
- (2) Lee, J. H.; Huh, Y. M.; Jun, Y.; Seo, J.; Jang, J.; Song, H. T.; Kim, S.; Cho, E. J.; Yoon, H. G.; Suh, J. S.; Cheon, J. *Nature Medicine* 2007, 13, 95.
- (3) Oo, M. K. K.; Yang, X.; Du, H.; Wang, H. *Nanomedicine* 2008, 3, 777.
- (4) Qian, H. S.; Guo, H. C.; Ho, P. C. L.; Mahendran, R.; Zhang, Y. *Small* 2009, 5, 2285.
- (5) Couleaud, P.; Morosini, V.; Frochet, C.; Richeter, S.; Raehm, L.; Durand, J. O. *Nanoscale* 2010, 2, 1083.
- (6) Hah, H. J.; Kim, G.; Lee, Y. E. K.; Orringer, D. A.; Sagher, O.; Philbert, M. A.; Kopelman, R. *Macromolecular Bioscience* 2011, 11, 90.
- (7) Vallet-Regi, M. *Chemistry-a European Journal* 2006, 12, 5934.
- (8) Choi, H. S.; Liu, W.; Misra, P.; Tanaka, E.; Zimmer, J. P.; Ipe, B. I.; Bawendi, M. G.; Frangioni, J. V. *Nature Biotechnology* 2007, 25, 1165.
- (9) Poland, C. A.; Duffin, R.; Kinloch, I.; Maynard, A.; Wallace, W. A. H.; Seaton, A.; Stone, V.; Brown, S.; MacNee, W.; Donaldson, K. *Nature Nanotechnology* 2008, 3, 423.
- (10) Derfus, A. M.; Chan, W. C. W.; Bhatia, S. N. *Nano Letters* 2004, 4, 11.
- (11) Park, J. H.; Gu, L.; von Maltzahn, G.; Ruoslahti, E.; Bhatia, S. N.; Sailor, M. J. *Nature Materials* 2009, 8, 331.
- (12) Popplewell, J. F.; King, S. J.; Day, J. P.; Ackrill, P.; Fifield, L. K.; Cresswell, R. G.; Di Tada, M. L.; Liu, K. *Journal of Inorganic Biochemistry* 1998, 69, 177.
- (13) Lin, W. S.; Huang, Y. W.; Zhou, X. D.; Ma, Y. F. *Toxicology and Applied Pharmacology* 2006, 217, 252.

- 1
2
3 (14) Wottrich, R.; Diabate, S.; Krug, H. F. *International Journal of Hygiene and*
4
5
6 *Environmental Health* 2004, 207, 353.
7
8 (15) Tang, L.; Fan, T. M.; Borst, L. B.; Cheng, J. J. *Acs Nano* 2012, 6, 3954.
9
10 (16) Tada, D. B.; Vono, L. L. R.; Duarte, E. L.; Itri, R.; Kiyohara, P. K.; Baptista, M. S.;
11
12 Rossi, L. M. *Langmuir* 2007, 23, 8194.
13
14 (17) Giri, S.; Trewyn, B. G.; Stellmaker, M. P.; Lin, V. S. Y. *Angewandte Chemie-*
15
16 *International Edition* 2005, 44, 5038.
17
18 (18) Rosenholm, J. M.; Peuhu, E.; Eriksson, J. E.; Sahlgren, C.; Linden, M. *Nano*
19
20 *Letters* 2009, 9, 3308.
21
22 (19) Tu, H. L.; Lin, Y. S.; Lin, H. Y.; Hung, Y.; Lo, L. W.; Chen, Y. F.; Mou, C. Y.
23
24 *Advanced Materials* 2009, 21, 172.
25
26 (20) Trewyn, B. G.; Whitman, C. M.; Lin, V. S. Y. *Nano Letters* 2004, 4, 2139.
27
28 (21) Agostini, A.; Mondragón, L.; Bernardos, A.; Martínez-Máñez, R.; Marcos, M. D.;
29
30 Sancenón, F.; Soto, J.; Costero, A.; Manguan-García, C.; Perona, R.; Moreno-Torres, M.;
31
32 Aparicio-Sanchis, R.; Murguía, J. R. *Angewandte Chemie International Edition* 2012, 51,
33
34 10556.
35
36 (22) Coll, C.; Mondragón, L.; Martínez-Máñez, R.; Sancenón, F.; Marcos, M. D.; Soto,
37
38 J.; Amorós, P.; Pérez-Payá, E. *Angewandte Chemie International Edition* 2011, 50, 2138.
39
40 (23) Li, Z.; Barnes, J. C.; Bosoy, A.; Stoddart, J. F.; Zink, J. I. *Chemical Society*
41
42 *Reviews* 2012, 41, 2590.
43
44 (24) Yang, P.; Gai, S.; Lin, J. *Chemical Society Reviews* 2012, 41, 3679.
45
46 (25) Vivero-Escoto, J. L.; Slowing, I. I.; Wu, C.-W.; Lin, V. S. Y. *Journal of the*
47
48 *American Chemical Society* 2009, 131, 3462.
49
50 (26) Chu, Z. Q.; Huang, Y. J.; Tao, Q.; Li, Q. *Nanoscale* 2011, 3, 3291.
51
52
53
54
55
56
57
58
59
60

1
2
3 (27) Severino, D.; Junqueira, H. C.; Gugliotti, M.; Gabrielli, D. S.; Baptista, M. S.

4
5
6 *Photochemistry and Photobiology* 2003, 77, 459.

7
8 (28) Lee, J. H.; Huh, Y. M.; Jun, Y.; Seo, J.; Jang, J.; Song, H. T.; Kim, S.; Cho, E. J.;

9
10 Yoon, H. G.; Suh, J. S.; Cheon, J. *Nature Medicine* 2007, 13, 95.

11
12 (29) Liu, Z.; Davis, C.; Cai, W. B.; He, L.; Chen, X. Y.; Dai, H. J. *Proceedings of the*

13
14
15 *National Academy of Sciences of the United States of America* 2008, 105, 1410.

16
17 (30) Choi, H. S.; Liu, W.; Misra, P.; Tanaka, E.; Zimmer, J. P.; Ipe, B. I.; Bawendi, M.

18
19
20 G.; Frangioni, J. V. *Nature Biotechnology* 2007, 25, 1165.

21
22 (31) Lee, C.-H.; Cheng, S.-H.; Wang, Y.-J.; Chen, Y.-C.; Chen, N.-T.; Souris, J.;

23
24
25
26
27
28
29
30
31
32
33
34
35
36
37
38
39
40
41
42
43
44
45
46
47
48
49
50
51
52
53
54
55
56
57
58
59
60
Chen, C.-T.; Mou, C.-Y.; Yang, C.-S.; Lo, L.-W. *Advanced Functional Materials* 2009,
19, 215.

(32) Rossi, L. M.; Silva, P. R.; Vono, L. L. R.; Fernandes, A. U.; Tada, D. B.;

Baptista, M. c. S. *Langmuir* 2008, 24, 12534.

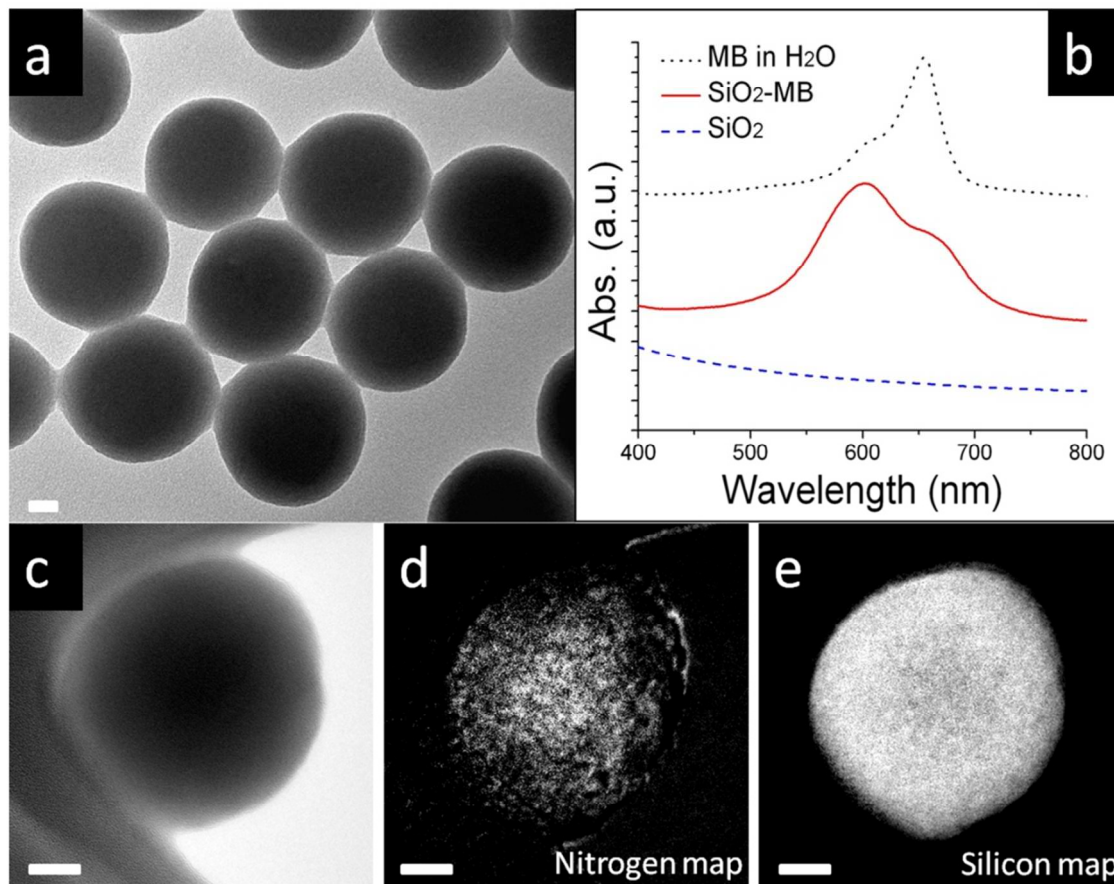


Figure 1. Characterizations of SiO₂-MB NPs. (a) Typical TEM image of the SiO₂-MB NPs; (b) Absorption spectra taken from pure MB, SiO₂-MB NPs and pure SiO₂ NPs in aqueous solutions; (c) Filtered bright field TEM image of single NP and the corresponding EELS maps of (d) Nitrogen and (e) Silicon. The scale bar is 20 nm.

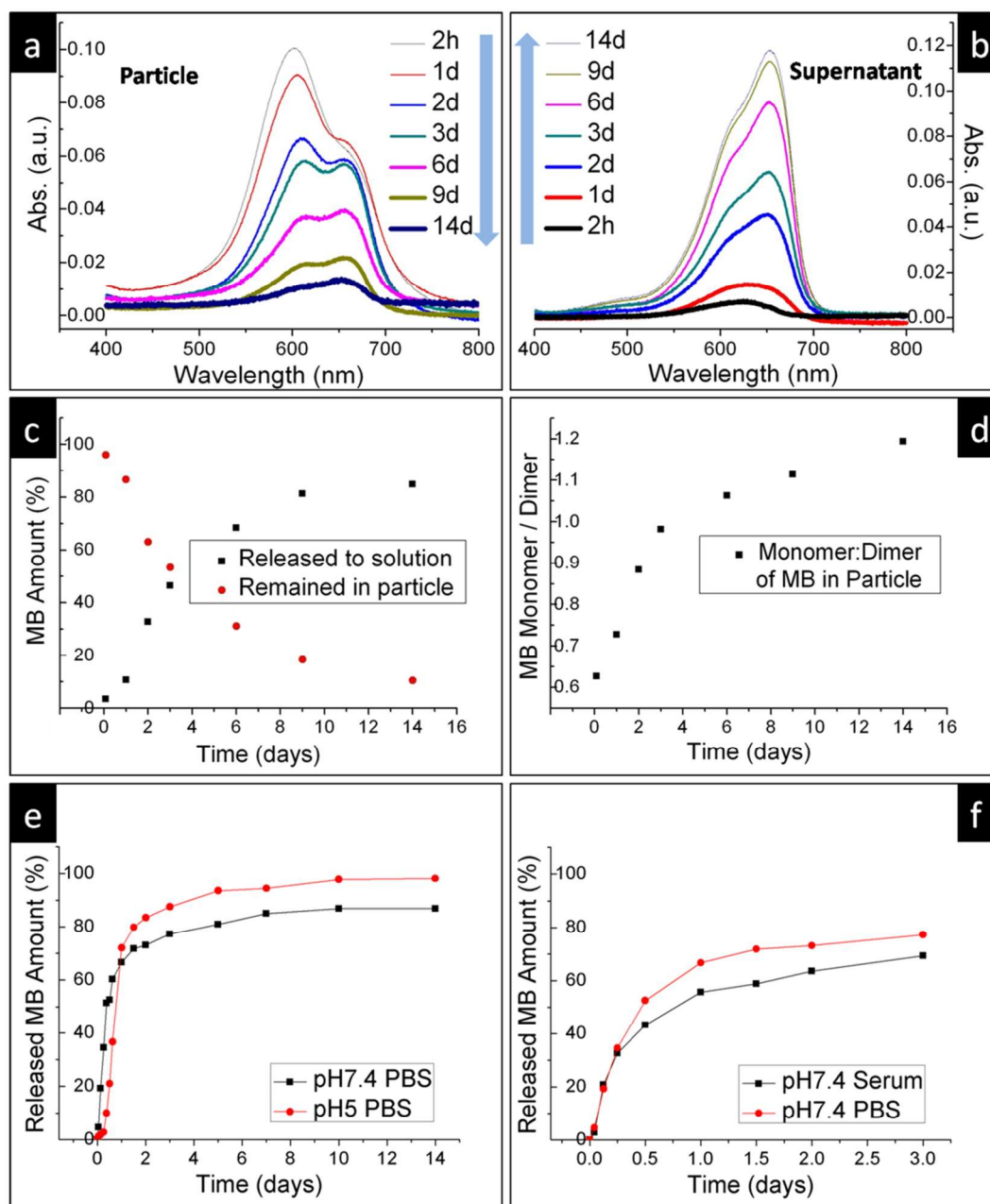


Figure 2. Release of MB from the SiO₂-MB NPs. Absorption spectra of (a) the SiO₂-MB NPs and (b) the supernatant after the NPs have been immersed in deionized water at room temperature for 2 hours, 1, 2, 3, 6, 9, and 14 days; (c) Evolution of the MB released into supernatant and MB remained in particle as a function of immersing duration (calculated from the absorption maximum peak intensity in a and b); (d) The ratio evolution of the MB monomer (665 nm) / dimer (600 nm) in the NPs as a function of immersing duration; Evolution of the MB released from the NPs as a function of the immersing duration (as calculated from the absorption maximum peak intensity of supernatant) investigated (e) in PBS with different pH values – pH 7.4 and pH 5, respectively; and (f) at pH 7.4, in different medium, i.e., serum and PBS at 37°C.

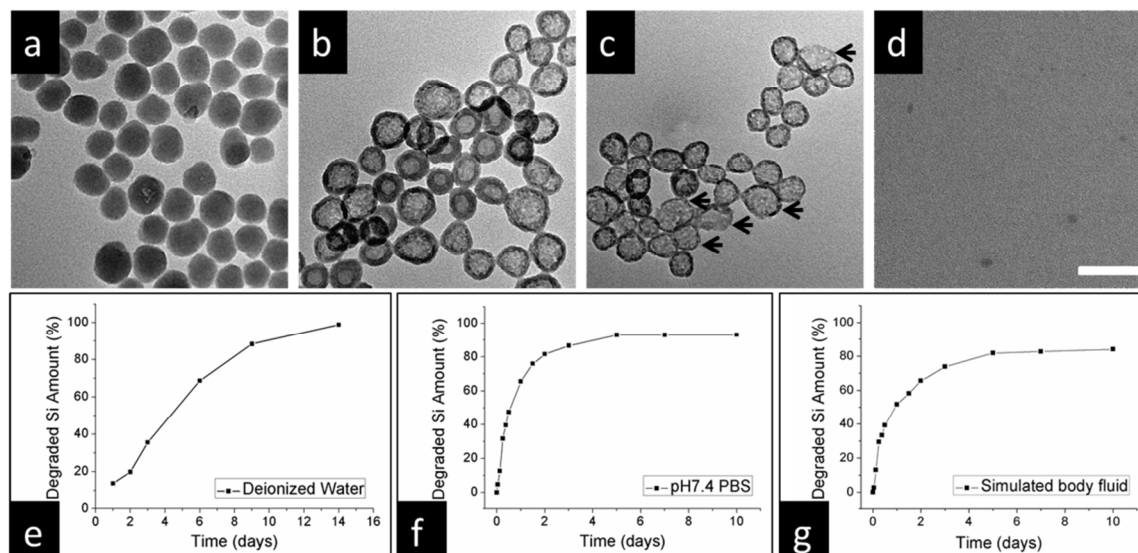


Figure 3. Carrier decomposition of SiO₂-MB NPs. Typical TEM images of the SiO₂-MB NPs after being immersed in deionized water for (a) 1 day; (b) 4 days; (c) 9 days; and (d) 14 days respectively. The scale bar is 100 nm; ICP-OES result of degraded silicon amount as a function of immersion duration in (e) deionized water at room temperature, (f) PBS (pH 7.4) and (g) simulated body fluid (with 50% FBS) at 37°C.

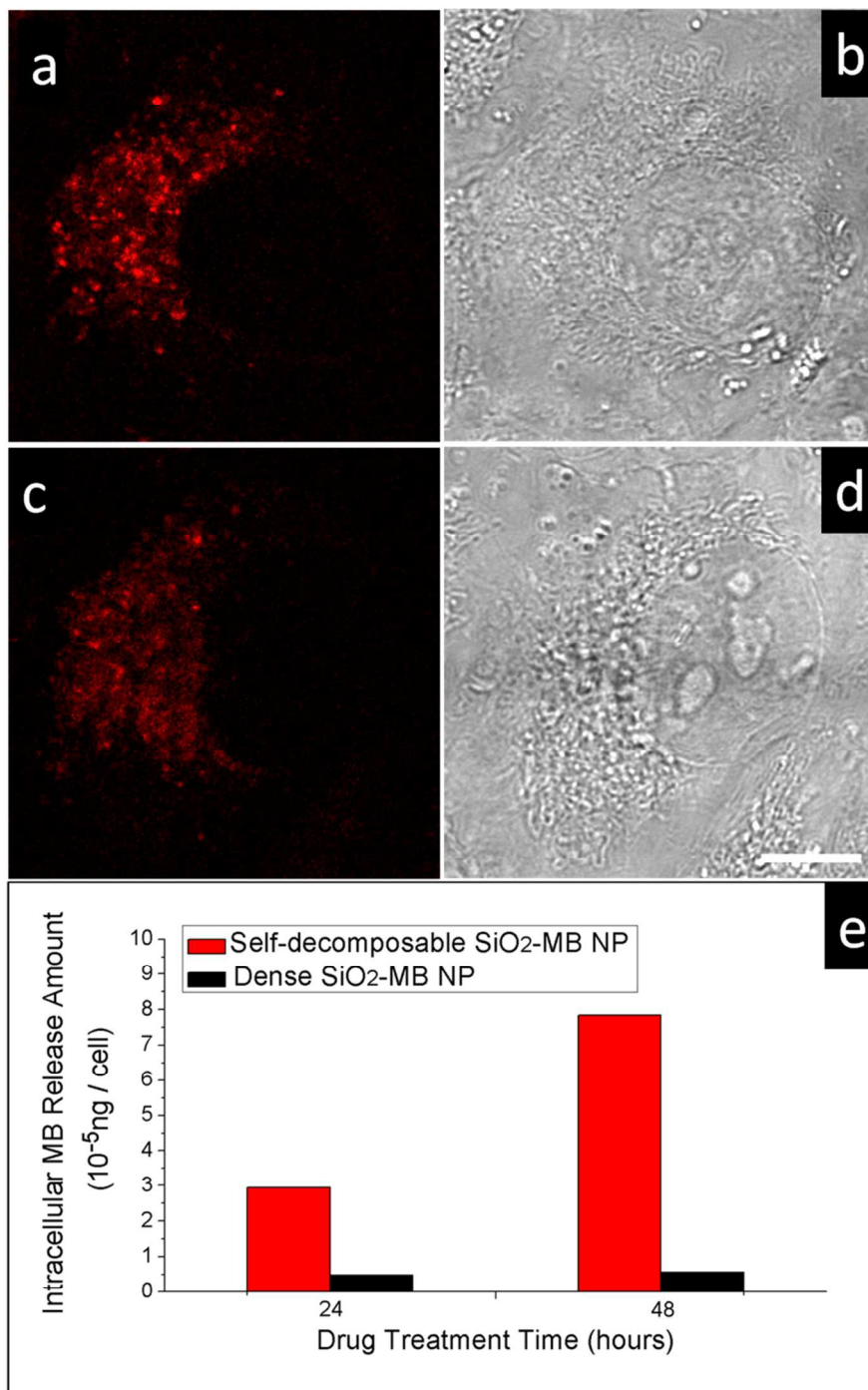


Figure 4. Observation of MB release in vitro. Confocal microscopy images of the H1299 cells treated with self-decomposable SiO₂-MB NPs for (a) 24 and (c) 48 hours (Fluorescence signal (red color) from MB with corresponding transmittance images ((b) and (d)) showing the morphologies of the specific cells). The scale bar is 10 μ m; (e) The amount of MB molecules released into cytoplasm after incubating the cells with self-decomposable SiO₂-MB NPs or dense SiO₂-MB NPs for 24 hours and 48 hours, respectively.

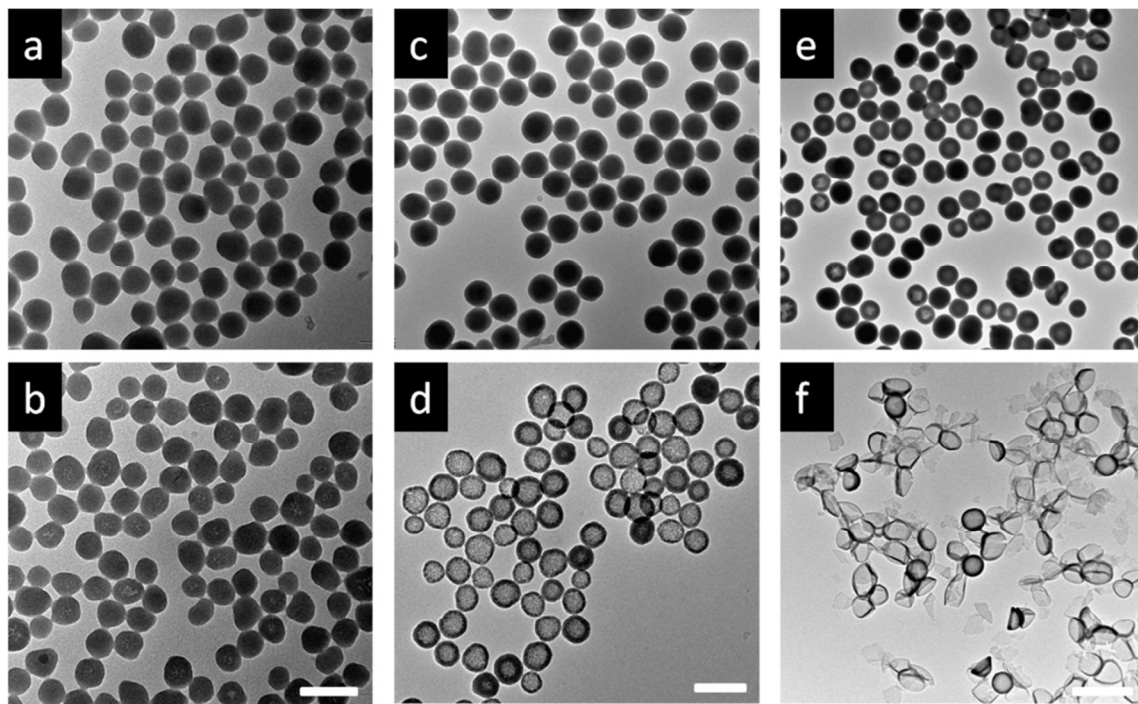


Figure 5. Controllable drug release and self-decomposition of SiO₂-MB NPs. TEM images of the freshly prepared SiO₂-MB NPs (top row) and those after being immersed in deionized water for 2 days (bottom row). (a,b) Sample M1; (c,d) Sample M2; and (e,f) Sample M3. The scale bar is 100nm for (a) and (b); 200 nm for (c) and (d); and 2 μm for (e) and (f).

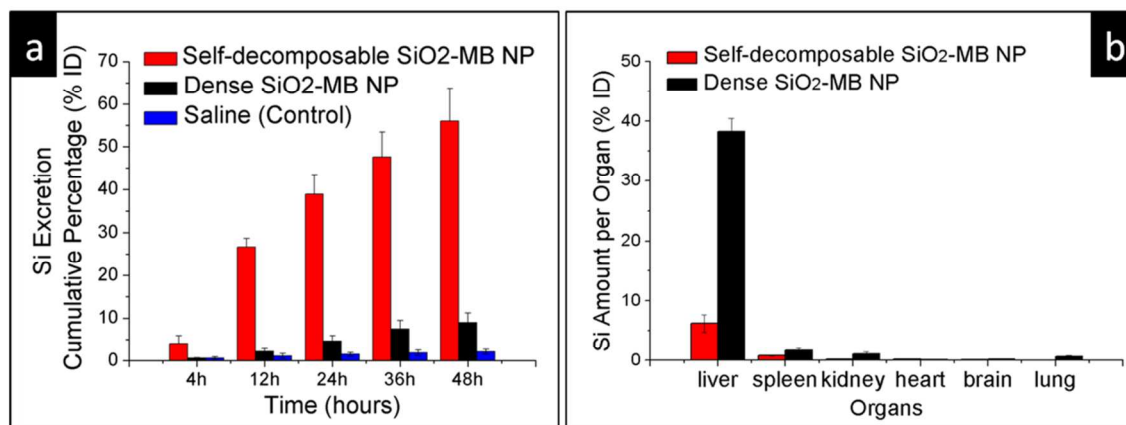


Figure 6. Urinary excretion and biodistribution of SiO₂-MB NPs. (a) ICP-OES analysis of Si amount in the urine of rats collected at 4 hours, 12 hours, 24 hours, 36 hours and 48 hours after injection of self-decomposable, dense SiO₂-MB NPs or saline (as the control); (b) ICP-OES analysis of Si amount in the organs of rats collected at 48 hours after injection of self-decomposable and dense SiO₂-MB NPs. The percentages are calculated by the average amount of Si detected compared to the total injection amount of SiO₂-MB NPs. Data are presented with Mean \pm SEM, n=3.

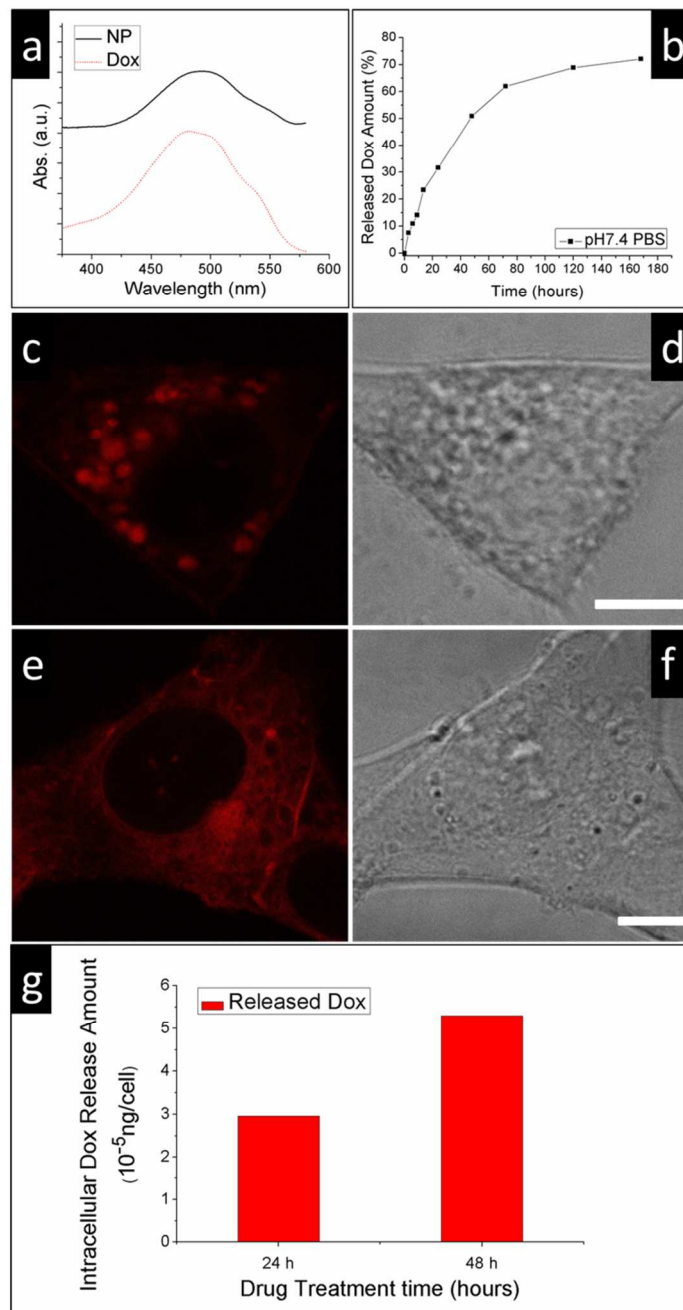


Figure 7. (a) Absorption spectrum (black solid line) showing the successful incorporation of Dox in the NPs. The red dashed line gives the characteristic absorption of pure Dox in aqueous solutions; (b) Evolution of the Dox released from the NPs as a function of immersing duration (calculated from the absorption maximum peak intensity of supernatant) investigated in pH 7.4 PBS at 37°C; (c) Confocal microscopy images of the cells treated with the NPs for 24 hours and (e) 48 hours (Fluorescence signal (red color) from Dox with corresponding transmittance images ((d) and (f)) showing the morphologies of the specific cells). The scale bar is 7.5 μ m; (g) Amount of Dox released to cytoplasm after incubating the cells with NPs for 24 hours and 48 hours.

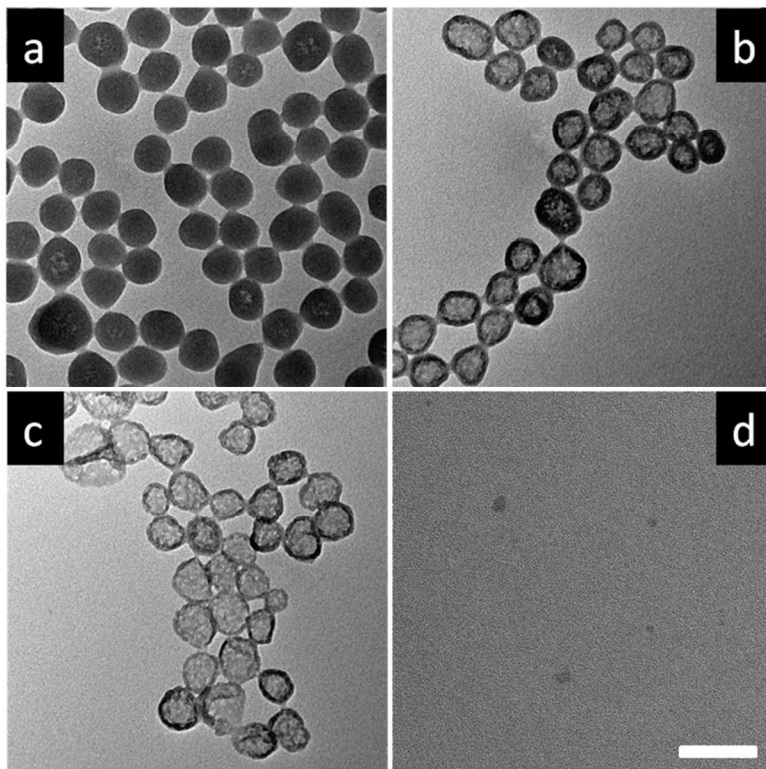


Figure 8. Morphological change of the Dox incorporated NPs. TEM images taken after the NPs' being immersed in deionized water for (a) 1 day (b) 4 days (c) 9 days and (d) 14 days, respectively. The scale bar is 100 nm.

Table of Contents

